Impact of Polymerization Protocol on Structure-Property Relationships of Entirely Lipid-Derived Poly(ester urethane)s

Shegufta Shetranjiwalla, Shaojun Li, Laziz Bouzidi and Suresh S. Narine*

Trent Centre for Biomaterials Research, Departments of Physics and Astronomy and Chemistry, Trent University, Ontario, Canada

Received October 08, 2016; Accepted December 31, 2016

ABSTRACT: The impact of polymerization protocol on phase structure and properties of entirely lipid-derived thermoplastic poly(ester urethane)s (TPEU)s was investigated. The TPEUs were synthesized from 1,7-heptamethylene diisocyanate, polyester diols and 1,9-nonanediol (ND) as chain extender. A two-stage polymerization method was used to prepare two TPEUs; one in which ND was added in the first stage of polymerization as part of the prepolymer and another in the second stage after the prepolymer was formed. Two very different morphologies exhibiting different degrees of phase separation were obtained, driven by the sequence of addition of the chain extender. The incorporation of the chain extender in the prepolymer resulted in a TPEU with a narrow hard segment distribution, enhanced urethane-urethane hydrogen bonding and higher molecular weight. The hydrogen bond density, degree of crystallinity, glass transition temperature and mechanical properties of the TPEUs were directly related to the degree of phase separation and hence polymerization protocol.

KEYWORDS: Renewable resources, segmented thermoplastic polyurethanes, hydrogen bond density, phase separation, biobased polymers

1 INTRODUCTION

Segmented thermoplastic polyurethanes (TPU)s are an interesting class of copolymers consisting of alternating "soft" and "hard" segment blocks linked together via covalent bonds [1]. In thermoplastic poly(ester urethane) (TPEU), the polyester serves as the soft segment and the polyurethane as the hard segment. Diol or diamine chain extenders are used to alternate with the diisocyanate and form *two-phase* structures in contrast to the *one-phase* or mixed phase polyurethanes which are synthesized without chain extenders [2]. The nature of building blocks and synthesis and polymerization conditions allow for considerable versatility in the design of the microphase morphology and phase structure of TPEUs, and therefore for significant control over the material properties [3]. The phase structure in segmented TPEUs is determined by several factors such as the ratio of the hard and soft segments in the copolymer, particularly hydrogen bonding [3]. For example, the hydrogen bonding between urethane-urethane improves the phase separation [4, 5], whereas hydrogen bonding between urethane and ester groups in the soft segments favors phase mixing, adversely affecting tensile properties [6, 7].

Recently, vegetable oils and their derivatives have gained considerable interest as precursors for a wide range of materials, including TPEUs [8]. Although attractive because of their renewability and positive environmental impact, the existing biobased TPEUs do not compete on a performance and economic basis with their petroleum equivalents. Unlike with partial replacement, such as with lipid-based diol [5] or diisocyanate [9], where some success was achieved, so far TPEUs made entirely from lipids demonstrated poor mechanical properties, particularly very low extension at break. This is attributed to their low molecular weight and insufficient phase separation [10, 11]. These limitations are design related and can be mitigated with an educated selection of constituents, discerning synthesis and polymerization protocols [12]. The phase separation of TPEUs can be improved by increasing the hydrogen bond density through a judicious arrangement of chain extenders [1]. The chain extenders may be added to the diisocyanate and the macrodiol in a one- or two-stage synthesis route. The one-shot polymerization method produces mixed phase TPEUs; whereas, the two-stage method

*Corresponding author: sureshnarine@trentu.ca

DOI: 10.7569/JRM.2017.634102

produces a more or less separated two-phase system of narrowly distributed urethane and polyester segments depending on reaction control [9, 13, 14].

The present work is a continuation of previous research efforts targeted at preparing segmented TPEUs from vegetable oil derivatives. In the first study, hard segments made of 1,7-heptamethylene diisocyanate (HPMDI) and 1,9-nonanediol (ND) chain extender, both derived from vegetable oil, were combined with petroleum-based polyethylene adipate diol soft segments to produce TPEUs with mechanical properties comparable to existing petroleum-based counterparts [9]. In the second study, synthesis conditions using stoichiometric imbalance methods were successfully optimized to produce *one-phase* entirely lipid-derived TPEUs with high molecular weight and improved strain at break. The TPEUs were synthesized from long-chain (C27) polyester diols (PEDs) prepared by a novel induced stoichiometric imbalance method as soft segments and HPMDI [15]. In the present work a chain extender (ND) was incorporated via a two-stage polymerization process to control the urethane hard segment distribution and hydrogen bond density in the entirely lipid-derived TPEUs from PEDs and HPMDI. Two *two-phase* TPEUs were synthesized with PEDs prepared by the novel induced stoichiometric imbalance method [15] and HPMDI, and compared to TPEU PU2.1-24h, a *one-phase* TPEU previously prepared without a chain extender by the single-stage polymerization method [15]. The solubility, phase separation and thermal and mechanical properties of the *two-phase* TPEUs are detailed.

2 EXPERIMENTAL

2.1 Materials

Stannous octoate ($Sn(Oct)_2$) (98%), dibutylamine (98%), 1,9-nonanediol (ND), calcium hydride (98%), anhydrous tetrahydrofuran (THF), calcium hydride (98%), N-methyl-2-pyrrolidone (NMP), 1,3-dimethyl-2-imidazolidinone (DMI), dimethylsulfoxide (DMSO) and diethyl ether were purchased from Sigma-Aldrich (Oakville, Ontario, Canada). Chloroform ($CHCl_3$), methanol and dimethylformamide (DMF) were obtained from ACP Chemicals Inc. (Montreal, QC, Canada). All reagents except DMF and THF were used as obtained. DMF was dried overnight over calcium hydride followed by vacuum distillation (~300 Torr). THF was distilled after drying overnight over 4A molecular sieves. The polyester diols (PEDs, molecular weight 2000 $gmol^{-1}$) were synthesized from oleic acid-derived 1,9-nonanedioic acid (azelaic acid) and ND as described previously [15]. 1,7-heptamethylenediisocyanate (HPMDI, 97%, 180 $gmol^{-1}$) was synthesized from azelaic acid according to a previously reported procedure [16].

2.2 Characterization Techniques

Solubility tests were conducted on TPEU samples after they were purified and dried under vacuum until constant weight. Tests were performed in $CHCl_3$, THF, DMF, NMP, DMI and DMSO. The sample (1 mg of TPEU in 1 mL of solvent) was stirred for 30 min and left in the solvent for 2 days. The sample was then brought to the boiling point of the solvent at least three times for at least 5 min each. In DMF, samples were refluxed for 15 min.

Fourier transform infrared spectroscopy (FTIR) was performed on a Thermo Scientific Nicolet 380 FTIR spectrometer (Thermo Electron Scientific Instruments, LLC, USA) equipped with a PIKE MIRacle™ attenuated total reflectance (ATR) system (PIKE Technologies, Madison, WI, USA). The sample was placed onto the ATR crystal area and held in place by the pressure arm. The spectrum was acquired in the 400–4000 cm^{-1} scanning range using 64 scans at a resolution of 4 wavenumbers. All spectra were recorded at ambient temperature. The analysis of the carbonyl stretching region was performed as described for other polyurethanes [17, 18]. The 1780 cm^{-1} to 1660 cm^{-1} region was fitted with three Gaussians corresponding to the peaks of the disordered (~1715 cm^{-1}) and ordered (~1690 cm^{-1}) hydrogen-bonded, and free (~1732 cm^{-1}) carbonyl stretching after baseline correction using OriginPro (version 9.2, 2015) software. An iterative least-squares method was used to obtain the best fit. The residuals of the fit were all better than 2%.

The carbonyl hydrogen bonding index (R, Equation 1) was determined as the ratio of the intensities of the normalized hydrogen-bonded peaks to the free carbonyl stretching peak. The degree of phase separation (DPS, Equation 2) was calculated from R [19].

$$R = \frac{C_{bonded} \times \varepsilon_{bonded}}{C_{free} \times \varepsilon_{free}} \approx \frac{A_{bonded}}{A_{free}} \quad (1)$$

$$DPS = \frac{C_{bonded}}{C_{bonded} + C_{free}} = \frac{R}{R+1} \quad (2)$$

where A_{bonded} and A_{free} are the absorbance of hydrogen-bonded and free carbonyl peaks, C_{bonded} and C_{free} are the concentrations and ε_{bonded} and ε_{free} are the extinction coefficients. Note that in Equation 1, although slightly different due to the wide distribution of hydrogen bond strengths, $\frac{\varepsilon_{bonded}}{\varepsilon_{free}}$ has been set to 1 following Seymour *et al.* [18].

Scanning electron microscopy (SEM) images of the TPEUs were obtained with a Phenom ProX apparatus (Phenom-World, The Netherlands) at an accelerating voltage of 15 kV and map intensity. Uncoated thin rectangular samples were fixed to the charge reduction sample holder with conductive tape. Composite images were captured using the Automated Image Mapping software (Phenom-World, The Netherlands).

Thermogravimetric analysis (TGA) was carried out on a Q500 TGA model (TA Instruments, Newcastle, DE, USA) under 40 mL/min balance purge flow and 60 mL/min sample purge flow of dry nitrogen. Approximately 9.0–10.0 mg of sample was loaded in an open TGA platinum pan that was equilibrated at 25 °C and then heated to 600 °C at 10 °C/min.

Films for tensile testing and dynamical mechanical analysis were prepared on a Carver 12-ton hydraulic heated bench press (Model 3851-0, Carver, Inc., Wabash, IN, USA). The dry sample was melt pressed at 150 °C and cooled at 5 °C/min down to room temperature (RT = 21 °C) and cast into dumbbell- and rectangular-shaped films of thickness 0.60 ± 0.25 mm.

The TPEU films were measured at RT by uniaxial tensile testing using a texture analyzer (Texture Technologies Corp., NJ, USA) equipped with a 2 kg load cell following the ASTM D882 procedure. The sample was stretched at a rate of 5 mm/min from a gauge of 35 mm. The reported results are the average and standard deviation of at least four specimens.

Wide-angle X-ray diffraction (WAXD) measurements were performed on a PANalytical Empyrean diffractometer (PANalytical B.V, Lelyweg, The Netherlands) equipped with a filtered CuKα (λ = 1.540598 Å) radiation source and PIXcel^{3D} detector used in line-scanning mode. The XRD patterns were recorded between 3 and 50° (2θ) in 0.026 steps. The procedure was automated and controlled by PANalytical Data Collector (V 3.0c) software. The data analysis was carried out using PANalytical X'Pert HighScore 3.0.4 software. The percentage degree of crystallinity (X_C, Equation 3) was estimated according to a known procedure [20].

$$X_C = 100 * \frac{A_C}{A_C + A_A} \quad (3)$$

where A_C is the area under the crystal diffraction peaks and A_A is the area under the amorphous halo. The amorphous contribution was fitted with two lines centered at 4.0 Å and 4.7 Å as usually done for semicrystalline polymers [21, 22].

Dynamical mechanical analysis (DMA) was performed on a Q800 model DMA (TA Instruments, New Castle, DE, USA) equipped with a liquid nitrogen cooling system. The pristine samples were thermally processed into films of rectangular shape (17.5 mm × 10 mm × 0.6 mm). Measurements were performed under the flexural oscillation mode following ASTM E1640 standard. The oscillation amplitude and frequency were fixed at 15 µm and 1 Hz, respectively, which is a sufficiently small deformation applied slowly so that the materials would remain in the linear viscoelastic region [23]. The sample was equilibrated at −90 °C for 5 min then heated at 2 °C/min to 40 °C. The samples maintained their dimensional integrity and thermoplastic nature and did not show any damage. The data was analyzed with TA Instruments Universal Analysis 2000 software.

Differential scanning calorimetry (DSC) measurements were carried out on the Q200 model (TA Instruments, Newcastle, DE, USA) following ASTM D3418. The sample (5.0–6.0 ± 0.6 mg) was weighed from the films prepared for DMA analysis and run in hermetically sealed aluminum pans under a dry nitrogen gas atmosphere. The sample was first heated to 180 °C at 10 °C/min (referred to as the 1st heating cycle) and held at that temperature for 5 min to erase thermal history and then cooled to −80 °C at 5 °C/min. The sample was subsequently heated to 180 °C at 10 °C/min (referred to as the 2nd heating cycle). The heating cycle measurements were performed in the modulation mode with modulation amplitude of 1 °C/min and a period of 60 s.

2.3 Synthesis of Segmented TPEUs

Two segmented TPEUs, coded ND-A and ND-B, were prepared with PED-3h (the molecular weight controlled PED prepared by inducing stoichiometric imbalance at three hours) [15], HPMDI and ND in the presence of $Sn(Oct)_2$ catalyst using the two-step polymerization method (Scheme 1). For ND-A, the chain extender was added in the second stage of polymerization after the HPMDI-PED-HPMDI prepolymer was formed (*Method* A, Scheme 1a), and for ND-B, the chain extender was added in the first stage of polymerization as part of the HPMDI-ND-HPMDI prepolymer (*Method* B, Scheme 1b). In both cases, the NCO:OH ratio was fixed at 1:1. The polymerization recipes and yields of ND-A and ND-B and PU2.1-24h for comparison are provided in Table 1.

Synthesis of ND-A (Scheme 1a): In the prepolymer of method A, excess HPMDI (0.63 g, 3.5 mmol) was dissolved in 6.3 mL of DMF in a round-bottom flask fitted with a thermometer and stirred under an inert atmosphere. The PED-3h (1.65 g, 0.9 mmol) and catalyst ($Sn(Oct)_2$, 0.07g, 0.16 mmol) were dissolved in 16.5 mL of DMF and then added to HPMDI through an addition funnel. The reaction was constantly stirred (600 rpm) at 85 °C for 5 h to form

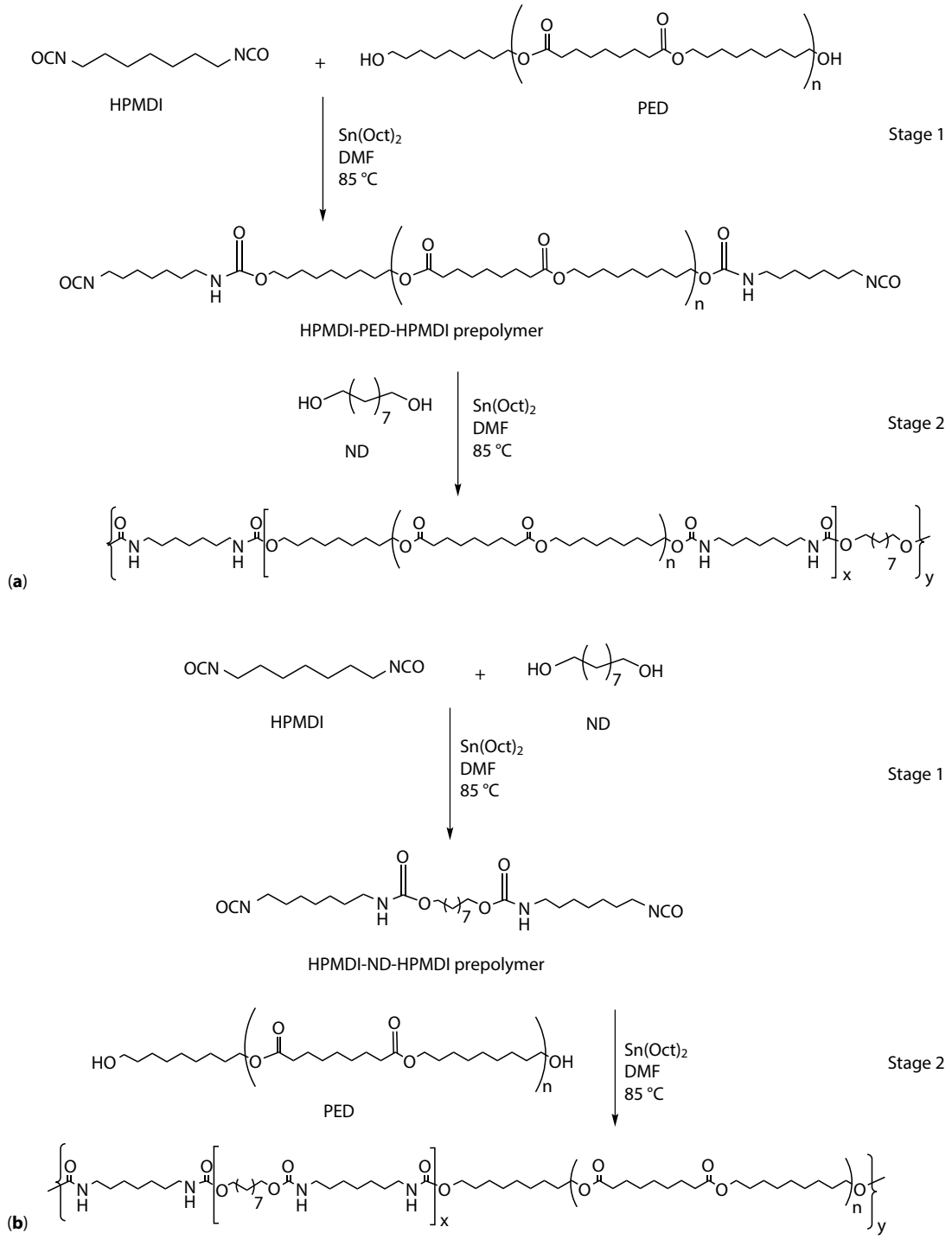

Scheme 1 Two-stage synthesis of TPEUs: (**a**) synthesis of ND-A, and (**b**) synthesis of ND-B.

HPMDI-PED-HPMDI prepolymer. In the second step, the chain extender (ND, 1.7 mmol) and catalyst ($Sn(Oct)_2$, 0.0064 g) were dissolved in 1.7 mL of DMF and added to the prepolymer. The reaction was continued at 85 °C for another 19 h under inert conditions with constant stirring at 400 rpm to achieve ND-A.

Synthesis of ND-B (Scheme 1b): *Method* B differed from *Method* A only in the sequence of addition of reactants. In the prepolymer of method B, excess HPMDI (0.63 g, 3.5 mmol) was dissolved in 6.3 mL of DMF and stirred at 85 °C. The chain extender (ND, 1.7 mmol) and catalyst ($Sn(Oct)_2$, 0.0064 g) dissolved in 1.7 mL of DMF was added to HPMDI from a dropping funnel under

Table 1 Recipe for the polymerization and the yield (%) of the TPEUs. The ratios of HPMDI (1,7-heptamethylene diisocyanate), ND (1,9-nonanediol, chain extender) and PED (polyester diol) used in the synthesis are molar.

Polymerization method	TPEU	Step 1			Step 2		
		HPMDI	ND	PED	ND	PED	Yield
A	ND-A	2.1	0	1.1	1.0	0	75
B	ND-B	2.1	1.0	0	0	1.1	80
One-shot	PU2.1-24h	2.1	–	1	–	–	82

constant stirring and reacted for 5 h to form HPMDI-ND-HPMDI prepolymer. In the second step, PED (1.65 g, 0.9 mmol) and catalyst ($Sn(Oct)_2$, 0.07g, 0.17 mmol), both dissolved in 16.5 mL of DMF, were added to the HPMDI-ND-HPMDI prepolymer. The reaction was continued for another 19 h under inert conditions with constant stirring at 400 rpm to achieve ND-B.

The polymers were precipitated from excess water and dried under vacuum until constant weight. They were purified by soaking in chloroform (10 mL/g) for one hour and washed with excess methanol. The structure was confirmed by FTIR (Figure S1 provided in the Supporting Information). The purified samples were melt-pressed into films for DMA and tensile measurements.

2.4 Synthesis of One-Phase TPEU

The one-phase PU2.1-24h was synthesized from HPMDI and PED-3h by the one-shot polymerization method using a previously reported procedure [15]. PED-3h was reacted in the presence of $Sn(Oct)_2$ catalyst and HPMDI in a single step using an NCO:OH ratio of 2.1:1. First, HPMDI (2.8 mmol, 0.5 g) was stirred in anhydrous DMF in a three-necked flask under N_2 atmosphere until dissolved. The PED (1.33 mmol, 2.66 g) and catalyst (20 mg/5mL) were also dissolved in anhydrous DMF and were added to the HPMDI via an addition funnel. The reaction was stirred at 85 °C and 400 rpm for 24 hours. The polymer was precipitated from water and dried under vacuum until constant weight. The polymer was purified by soaking in chloroform (10 mL/g) for one hour followed by washing with excess methanol and dried under vacuum.

3 RESULTS AND DISCUSSION

3.1 Solubility of the TPEUs

The solubility results of the segmented TPEUs in $CHCl_3$, THF, DMF, NMP, DMI and DMSO are shown in Table 2. The polarities of the solvents used in the experiment as indicated by their dielectric constants [24] are provided in Table 2. As shown in Table 2, ND-A, ND-B and PU2.1-24h were insoluble at room temperature in any of the solvents used, even the most polar ones such as DMF or DMSO. This behavior is attributed to the combination of strong van der Waals forces between the linear polyethylene-like structure of the TPEUs and high molecular weight. The alternating m, n polyurethane structure of ND-A and ND-B (where m=7 and n=9), present sequentially spaced aliphatic segments of sufficient length to generate the attractive forces which restrict the solubility of the final TPEUs. The (in)solubility of linear aliphatic PU materials obtained with difunctional species is not uncommon. It has been reported for other linear biobased as well as petroleum-based polyurethanes [25, 26]. At solvent boiling point, ND-B and PU2.1-24h were insoluble in all solvents; whereas, ND-A showed partial solubility in DMF and DMSO. This suggests that contrary to ND-B, which was insoluble in all solvents, the partially soluble ND-A probably had a lower molecular weight. Furthermore, as will be shown in Section 3.8, the tensile strength and elongation of ND-A were also lower than that of ND-B, which typically indicate a lower molecular weight polymer. The solubility results are of practical importance for TPEU applications requiring high solvent resistance.

Table 2 Solubility behavior of ND-A, ND-B and TPEU2.1-24h in solvents with varying polarity at their boiling points. I: Insoluble PS: Partially soluble.

Solvent	ε	ND-A	ND-B	PU2.1-24h
$CHCl_3$	4.85	I	I	I
THF	7.52	I	I	I
NMP	32.00	I	I	I
DMI	37.60	I	I	I
DMF	38.25	PS	I	I
DMSO	47.00	PS	I	I

3.2 FTIR and Hydrogen Bonding Index

Figure 1a, b shows the results of peak fitting of the 1660–1780 cm^{-1} region of the FTIR for ND-A and ND-B. The peak fitting result for PU2.1-24h [15] is provided in Figure 1c for comparison purposes. The carbonyl hydrogen bonding index (*R*, Equation 1), which

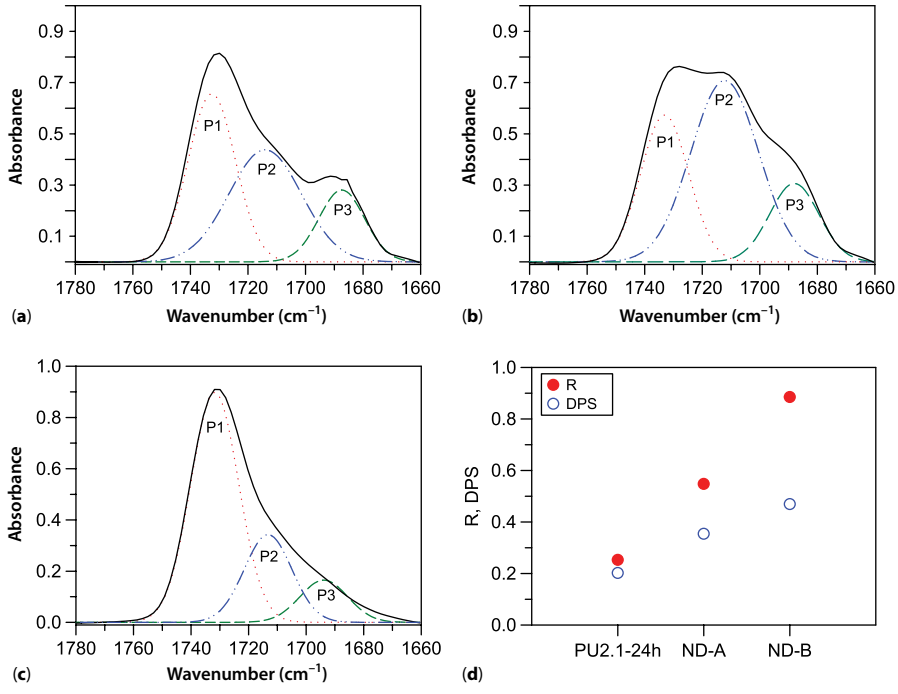

Figure 1 FTIR spectra of the carbonyl region of (**a**) ND-A, (**b**) ND-B and (**c**) PU2.1-24h. Dashed peaks are the results of the fit to Gaussians of the baseline corrected C=O stretching bands. P1: free, P2: disordered hydrogen-bonded and P3: ordered hydrogen-bonded carbonyl groups. (d) Hydrogen bond index (R, •) and degree of phase separation (DPS, ∘) of the TPEUs.

provides a measure of the increasing participation of the carbonyl groups in hydrogen bonding, and the degree of phase separation (DPS, Equation 2), which provides the measure of urethane-urethane interaction, are presented in Figure 1d. The variation of *R* and *DPS* values (filled and empty circles in Figure 1d, respectively) indicates an increase of the interurethane hydrogen bonding and suggests the improvement of phase separation from PU2.1-24h to ND-A and ND-B. The very low DPS value of PU2.1-24h indicates a high phase mixing associated with a random dispersion of urethane segments in the polyester matrix. The difference in DPS of ND-A and ND-B stems from the protocols used during prepolymer synthesis. Nonanediol (C9) as chain extender is expected to contribute with a lower hydrogen bond density in the hard segment unlike a short-chain diol such as butane diol (C4), typically used in the synthesis of TPEUs. Also, because nonanediol bears similarities in structure and polarity to the soft segment of the TPEU, it is not expected to establish a very strong phase separation. However, the sequence in which nonanediol was introduced during the prepolymer synthesis (protocols A and B), increased hydrogen bond density in the hard segment and the overall difference in polarity between the hard and soft phases, ending in a larger phase separation in ND-B than ND-A. Also, contrary to the aromatic diisocyanates, there is no electronegativity effect for the linear aliphatic HPMDI of the present work. If any, steric effect will also be negligible. Rather, the rate of reaction is governed by proximity effects arising from the molecular size of the diisocyanate-terminated prepolymers known to impact accessibility of the isocyanate groups for subsequent reaction [13, 14, 27]. The different molecular sizes of the prepolymers of ND-A and ND-B, predesigned in the first stage of polymerization, result in the different reactivity in the following second stage and the subsequent difference in molecular weight and yield. The better reactivity of ND-B and subsequent better polymer yield after precipitation compared to ND-A is attributable to a more favorable spatial distance between the two isocyanate groups in the HPMDI-ND-HPMDI prepolymers of ND-B compared to the HPMDI-PED-HPMDI prepolymer of ND-A (a minimum of 43 carbons versus 25 carbons). Moreover, during the polymerization of ND-A, the concentration of the more reactive HPMDI monomer available to react with ND was lower in stage two. Also, the concentration of available HPMDI was probably further reduced by the potential organotin catalyst-mediated fragmentation of the PED, upsetting the overall NCO:OH stoichiometric imbalance in this stage [15] and affecting the subsequent reaction with ND. This may explain the lower yield after precipitation (Table 1) and the lower molecular weight of ND-A compared to ND-B for which the concentration

of the monomer diisocyanate available to react with PED in the second step was higher. Furthermore, because the chain extender was sandwiched between diisocyanate segments, a larger sequence length of the urethane hard segment is formed in ND-B (repeating unit x, Scheme 1b). This promotes greater intermolecular hydrogen bonding between neighboring urethane segments and results in a narrowly distributed hard segment structure and improved phase separation. In contrast, a major portion of the diisocyanate in ND-A is sandwiched between two flexible PED chains (repeating unit x in Scheme 1a) and is considered to be a part of the soft segment [14], where it is more likely to participate in urethane-ester hydrogen bonding leading to increased phase mixing.

3.3 Scanning Electron Microscopy

Figures 2a–c show the SEM images of ND-A, ND-B and PU2.1-24h, respectively. As shown in Figure 2a and b, the surface morphology of the segmented TPEUs is constituted of protuberances (pointed to by a filled arrow in Figure 2b) separated by trough-like regions (pointed to by an empty arrow in Figure 2b), indicating a two-phase system. The prominent regions in the SEM images of Figure 2 indicate microstructures which are normally associated with the self-assembly of hydrogen bonded urethane hard phase; whereas, the trough-like regions are associated with the amorphous polyester chains and constitute the soft phase [28–30]. The average size of the microstructures increased from ~0.7 ± 0.2 μm for PU2.1-24h, to 1.2 ± 0.2 μm for ND-A and 2.3 ± 0.7 μm for ND-B, indicating an increase in urethane hard segment content and hydrogen bond density. ND-B showed much larger microstructures (Figure 2b) than ND-A (Figure 2a), indicating a larger size of the hydrogen bonded urethane phase. In contrast, PU2.1-24h displayed a wrinkled surface morphology (Figure 2c) with much smaller microstructures, a morphology commonly associated with the predominance of an amorphous phase [31]. The microstructures of PU2.1-24h show that the hard domains are dispersed in the soft matrix and reflect the FTIR results, which indicated the lowest DPS. One can note that the trough-like regions formed by amorphous polyester chains between the urethane microstructures are deepest in ND-B, indicating an improved interconnectedness and a distinct phase separation. Comparatively, SEM of ND-A showed much smaller microstructures indicative of less developed urethane hard segment domains. The surface morphology of ND-A is indicative of a higher phase mixing which is the direct result of the polymerization protocol (*Method* A, Scheme 1a). The SEM data show that urethane hard segment domains and phase separation were promoted by the addition of the chain extender and further by the polymerization protocol.

3.4 Thermal Degradation

Figures 3a and b show the DTG and TGA profiles, respectively, of ND-A, ND-B and PU2.1-24h. The corresponding degradation parameters are provided in Table S1 in the Supporting Information. Three weight loss steps at (280–300 °C), (390–400 °C) and (450 °C) corresponding to the degradation of the C-NH, C-O and the C-C bonds, respectively [32–34], are distinctly indicated by the TGA and DTG of the TPEUs. The TGA data confirm that the segmented TPEUs (ND-A and ND-B) had larger hard segments content than the one phase PU2.1-24h. In fact, the weight loss associated with the urethane and ester decomposition is in accordance with the initial formulation of the TPEUs where the amount of HPMDI (24.6%) used in ND-B

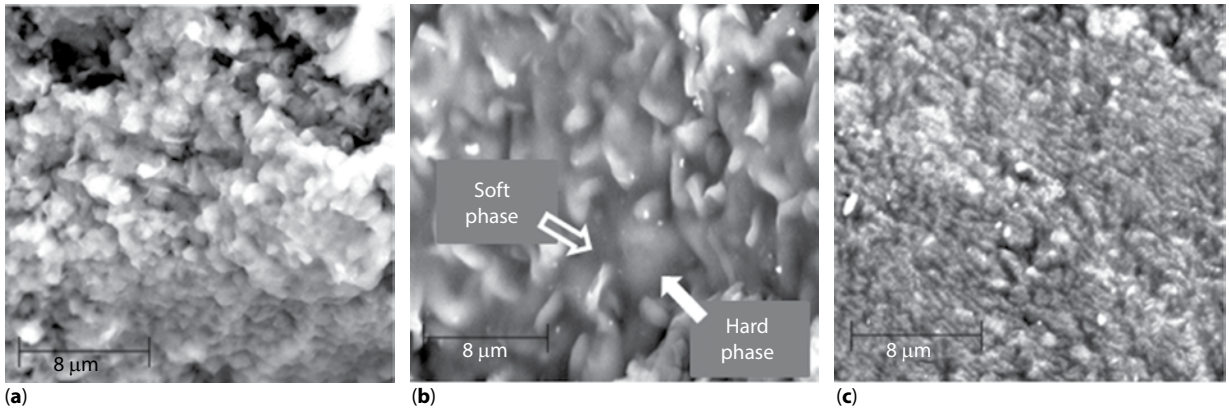

Figure 2 SEM micrographs for the segmented TPEUs (**a**) ND-A and (**b**) ND-B, and (**c**) PU2.1-24h.

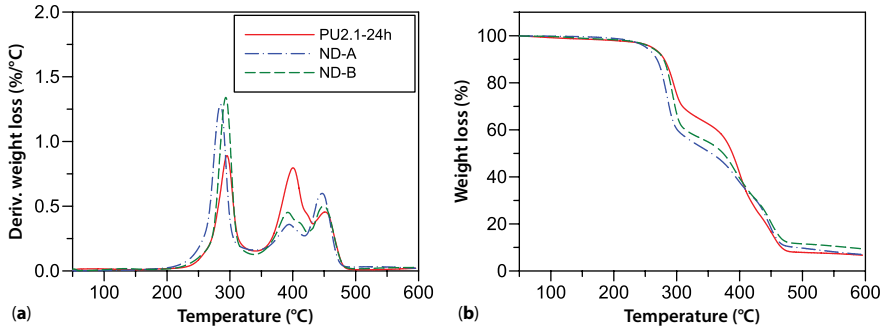

Figure 3 (**a**) Derivative TGA and (**b**) TGA curves for ND-A, ND-B and PU2.1-24h.

and ND-A was almost 1.5 times the amount used for PU2.1-24h (17.2%). ND-A and ND-B presented a similar degradation onset temperature (T_{on}^{d} ~ 258 °C), indicating that the thermal stability of the segmented TPEUs is independent of the extent of phase separation. PU2.1-24h presented a higher thermal stability with T_{on}^{d} at 271 °C, attributed to its higher polyester soft segment content and subsequent increased resistance to thermal scission of the crystalline polyethylene-like linear chain stacking [35, 36].

3.5 Thermal Transition Behavior

Figure 4 shows the second DSC heating cycles of ND-A and ND-B and PU2.1-24h. The corresponding melting parameters and glass transition temperatures are summarized in Table 3. The manifestation of two distinct melting transitions in the DSC thermograms of ND-A and ND-B (indicated by arrows, Figure 4) confirmed the *two-phase* structure of the segmented TPEUs. The endotherm at ~40 °C is attributable to the melting of the PED soft segment crystals and the endotherm at ~90 °C to the HPMDI-ND hard segment crystals [9]. In contrast, PU2.1-24h showed a unique endotherm at an intermediate temperature (~52 °C), indicative of the melting of PED-HPMDI segment crystallites of a co-continuous phase [15]. The improved degree of phase separation in the segmented TPEUs ND-A and ND-B was reflected in the decreased peak temperatures (T_m) and enthalpy (ΔH) of melting of the soft segments compared to the melting of the co-continuous phase of PU2.1-24h. This is explained by the increased phase separation of the polyester segments from the hydrogen-bonded urethane segments, and the resulting weaker attractions (van der Waals forces) in the soft segments of the segmented TPEUs as compared to the one-phase PU2.1-24h. The melting parameters are lower in ND-B than ND-A, indicating that a better separation of the soft segment phase from the hard segment phase occurs in ND-B. PU2.1-24h exhibits a higher T_m and ΔH, attributable to its phase-mixed

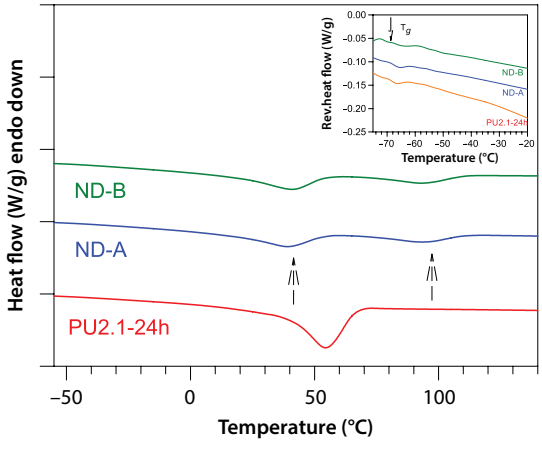

Figure 4 DSC thermograms obtained during the second heating cycle (10 °C/min) for the segmented TPEUs ND-A and ND-B, and one-phase PU2.1-24h. Inset is a zoom into the glass transition of the TPEUs.

Table 3 Thermal data obtained during the second heating cycle (10 °C/min) of the segmented TPEUs. T_m (°C) and ΔH (J/g): melting and enthalpy of melting, respectively. T_g (°C): glass transition temperature. The uncertainties attached to the characteristic temperatures and enthalpies are better than 2.9 °C and 2.1 J/g, respectively.

	Soft segment phase		Hard segment phase		
TPEU	T_m	ΔH	T_m	ΔH	T_g
ND-B	39.9	34.2	92.7	14.4	–71.6
ND-A	42.0	35.5	88.2	12.4	–67.0
	Co-continuous phase				
PU2.1-24h	52.4	53.4	–	–	–68.1

nature of urethane segments in the larger polyester matrix (83% versus 75% in ND-A and ND-B). The melting data of the hydrogen-bonded urethane segments can be related to the extent of the hard segment distribution in the segmented TPEU. The lower enthalpy

of ND-A hard segment crystallites compared to ND-B indicates a lower crystallinity ascribed to a lower hard segment hydrogen bond density. ND-A presented a lower value of T_m than ND-B, indicating smaller urethane hard segment domains. ND-A and PU2.1-24h, which share a similar structure of their amorphous soft segments corresponding to the one-shot polymerization protocol A followed, also show similar glass transition temperatures (T_g). ND-B exhibited the lowest T_g, attributed to the maximum soft segment chain mobility related to the superior phase separation associated with polymerization protocol B.

3.6 Crystal Structure

Figure 5 shows WAXD patterns of ND-A, ND-B and PU2.1-24h. The WAXD of the three TPEUs show a strong peak at 4.12 Å, medium peak at 3.79 Å and weaker peak at 3.02 Å, corresponding to the (110), (200) and (020) planes, respectively, of an orthorhombic sub-cell structure. Such an orthorhombic structure, denoted β', is associated with the packing of the polyester segments [37, 38] and is common in poly(ester) urethanes. ND-B displayed an extra weak peak at 4.41Å associated with the (100) plane of a monoclinic sub-cell, a crystal type observed in strongly hydrogen-bonded thermoplastic poly(ester urethanes) [9, 10] and aliphatic poly(ester amide)s (PEA)s [39], and is ascribed to the urethane or amide segment packing. The absence of detectable peaks of the monoclinic structure in the WAXD of ND-A, like PU2.1-24h indicate that their interurethane hydrogen bonding is not sufficiently strong to form distinct crystal structures. The high relative intensity of the peak at 4.41 Å in ND-B is an indication of a relatively high level of ordered urethane segments. The other characteristic peaks of the monoclinic form cannot be extracted from the WAXD of ND-B, probably because of the size and peculiar distribution of its urethane hard segment

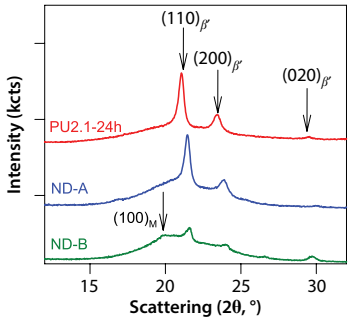

Figure 5 WAXD profiles of ND-A, ND-B and PU2.1-24h, measured at room temperature, showing the indexed reflection planes corresponding to different crystalline forms. β': Orthorhombic, M: Monoclinic

which constrain the soft segment packing, favoring the formation of amorphous regions. Such constraints are reflected in the larger amorphous halo in the WAXD spectrum of ND-B and its lower related crystallinity and in the lower melting temperature of its PED crystals comparatively to the polyester crystals of ND-A and PU2.1-24h (see T_m of the soft segments in Figure 4 and Table 3). These data corroborate the SEM and FTIR, pointing to the effectiveness of protocol B for polymerization of TPEUs to provide a higher degree of phase separation than protocol A.

The degree of crystallinity (*Xc*) as determined from the intensity of the crystal peaks to the total intensity of the WAXD signal was highest for PU2.1-24h (44%), followed by ND-A (22%), and lowest for ND-B (18%). PU2.1-24h presented the highest *Xc* comparatively to ND-A and ND-B because of its larger PED content. ND-B showed a lower *Xc* compared to ND-A due to its shorter soft segment blocks and the constraints imposed by its larger urethane segment structures on the soft segment packing owing to its specific polymerization protocol (protocol B).

3.7 Dynamic and Static Mechanical Properties

Figure 6a,b shows the storage and loss modulus versus temperature curves, respectively, of ND-A, ND-B and PU2.1-24h. The storage modulus recorded in the glassy region was highest for ND-B (3.87 ± 0.60 GPa), followed by ND-A (3.70 ± 0.04 GPa) then PU2.1-24h (3.52 ± 0.08), as one would expect from their decreasing hard segment content and associated hydrogen bonding density (R, in Figure 1d). In the rubbery and leathery regions, the storage modulus decreased consistent with their soft segment crystallinity level. PU2.1-24h shows a slightly higher retention of stored energy than ND-B and ND-A, attributed to the presence of urethane segments in the polyester soft segment matrix, i.e., high phase mixing (lowest DPS, Figure 1d). A single loss modulus peak was detected below room temperature for PU2.1-24h, ND-A and ND-B, attributed to the glass transition of the amorphous units of the TPEU soft segments. No glass transition was detected for the hard segments.

The glass transition (T_g), as determined at the peak maximum of the loss modulus curve, was −25.1 ± 0.7 °C for PU2.1-24h, a value that is close to that for ND-A (−23.2 ± 0.2 °C), indicating very close amorphous phase structures attributable to the one-shot method and the prepolymers of protocol A. The much lower T_g of ND-B (−28.7 ± 1.2 °C) can be ascribed to its more pronounced phase separation and greater purity of its polyester soft segments associated with the polymerization protocol B.

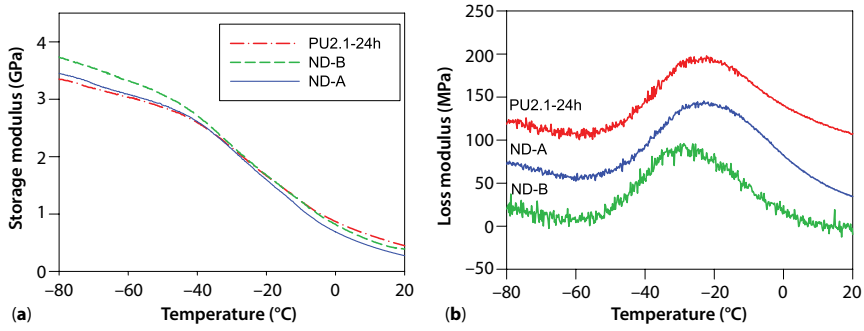

Figure 6 Viscoelastic properties of TPEUs (**a**) storage modulus and (**b**) loss modulus versus temperature curves of ND-A, ND-B and PU2.1-24h [15].

3.8 Tensile Properties

The stress-strain curves of PU2.1-24h, ND-A and ND-B are shown in Figure 7. The corresponding tensile data are provided in Table 4. In contrast to PU2.1-24h which displayed yielding followed by a drop in stress indicative of semicrystalline materials, ND-A and ND-B exhibited rubberlike stress-strain curves with no apparent yield point, characteristic of polymers with high phase separation [40]. ND-A and ND-B showed lower tensile strength and modulus compared to PU2.1-24h, attributed to their lower polyester segment crystallinity [41]. The higher tensile strength and modulus of PU2.1-24h compared to ND-A and ND-B is the result of its much higher polyester crystallinity. Incidentally, a linear trend for Young's modulus versus degree of crystallinity has been observed in linear polyethylene [42]. Also, as reported by Korley *et al.* [43] for aliphatic TPEUs with low hard segment content, the amorphous segments orient and crystallize under strain, acting as a stress-bearing phase which further increases the tensile strength. ND-B displayed the highest elongation at break (440 ± 52%), attributed to its higher degree of phase separation which provided well-developed reinforcing crystalline phase structures that serve as effective stress-bearing junctures. PU2.1-24h also exhibited high strain (353 ± 50%) (Table 4) attributed to the strain hardening typical of elastomers which is also visible in ND-B. Although, ND-A exhibited a smooth transition from the elastic to the plastic region associated with its improved phase separation, the presence of less developed hard segment domains and low molecular weight provided ineffective stress-bearing junctures, leading to reduced strain at break.

The strength and extensibility values obtained for ND-A and ND-B are superior to the entirely lipid-derived segmented TPUs without chain extender [11] and approach those of ultra-high molecular weight, partially lipid-derived TPEUs [9] prepared in our laboratories (ELD and PLD, respectively, in Table 4). The

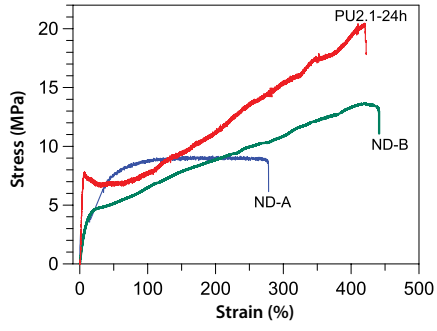

Figure 7 Stress-strain curves for ND-A, ND-B and PU2.1-24h [15].

Table 4 Mechanical properties of ND-A, ND-B and PU2.1-24h compared to TPEUs selected from the literature. Polyester grade thermoplastic (PGTE) synthesized from aliphatic diisocyanates. PGTE1: PEARLCOAT Activa D198K and PGTE2: PEARLTHANE D91F88 (Merquinza, Lubrizol, Ohio, USA). The uncertainties attached to ultimate tensile strength, Young's modulus and elongation at break for TPEUs synthesized in this study are the standard deviations of at least four runs and are better than 1.9 MPa, 31.5 MPa, and 51.6%, respectively.

TPEUs	Young's modulus (MPa)	Ultimate strength (MPa)	Maximum strain (%)
ND-A	123.6	8.4	236.5
ND-B	49.4	14.2	440.0
PU2.1-24h	253.5	18.2	353.4
ELD	–	21.0	39.0
PLD	83.0	22.8	543.0
PGTE1	–	25.0	455.0
PGTE2	–	23.0	388.0

mechanical properties of ND-A and ND-B also compare favorably with commercially available polyester grade TPEUs synthesized from aliphatic diisocyanates (PGTE 1 and 2 in Table 4).

4 CONCLUSIONS

Entirely lipid-derived segmented thermoplastic poly(ester urethane)s (TPEU)s with mechanical properties analogous to rubber were synthesized from oleic acid-derived polyester diols, 1,7-heptamethylene diisocyanate and 1,9-nonandiol. Phase separation, molecular weight, hydrogen bond density and thus hard segment distribution and crystallinity of the TPEUs were controlled by using a chain extender and by varying polymerization protocols. The study demonstrates that the polymerization procedure can be customized for both hydrogen bond density and phase separation. The TPEUs which were produced using this approach presented very high molecular weight, improved phase separation and physical properties. Their mechanical properties are superior to those of any other fully lipid-derived TPEUs reported in the literature and compare very favorably to commercial petroleum-based counterparts.

ACKNOWLEDGMENTS

We would like to thank the Ontario Soybean Growers/ Grain Farmers of Ontario, Elevance Renewable Sciences, Trent University, GPA-EDC, Ontario Ministry of Agriculture, Food and Rural Affairs, Industry Canada and NSERC for their financial support.

REFERENCES

1. M. Szycher, *Szycher's Handbook of Polyurethanes*, p. 41, CRC Press, Boca Raton,USA, (2012).
2. M. Szycher, *Szycher's Handbook of Polyurethanes*, CRC Press, Boca Raton, USA (1999).
3. I. Yilgör, E. Yilgör, and G.L. Wilkes, Critical parameters in designing segmented polyurethanes and their effect on morphology and properties: A comprehensive review. *Polymer* **58**, A1–A36 (2015).
4. D.J. Blundell, G. Eeckhaut, W. Fuller, A. Mahendrasingam, and C. Martin, Real time SAXS/stress–strain studies of thermoplastic polyurethanes at large strains. *Polymer* **43**, 5197–5207 (2002).
5. A. Saralegi, L. Rueda, B. Fernández-d'Arlas, I. Mondragon, A. Eceiza, and M. Corcuera, Thermoplastic polyurethanes from renewable resources: Effect of soft segment chemical structure and molecular weight on morphology and final properties. *Polym. Int.* **62**, 106–115 (2013).
6. S. Das, D.F. Cox, G.L. Wilkes, D.B. Klinedinst, I. Yilgor, E. Yilgor, and F.L. Beyer, Effect of Symmetry and H-bond strength of hard segments on the structure-property relationships of segmented, nonchain extended polyurethanes and polyureas. *J. Macromol. Sci. B.* **46**, 853–875 (2007).
7. B.K. Kim, S.Y. Lee, and M. Xu, Polyurethanes having shape memory effects. *Polymer* **37**, 5781–5793 (1996).
8. G. Lligadas, J.C. Ronda, M. Galia, and V. Cadiz, Renewable polymeric materials from vegetable oils: A perspective. *Mater. Today* **16**, 337–343 (2013).
9. S. Li, J. Jose, L. Bouzidi, A.L. Leao, and S.S. Narine, Maximizing the utility of biobased diisocyanate and chain extenders in crystalline thermoplastic segmented polyester urethanes: Effect of polymerization protocol. *Polymer* **55**, 6764–6775 (2014).
10. L. Hojabri, J. Jose, A.L. Leao, L. Bouzidi, and S.S. Narine, Synthesis and physical properties of lipid-based poly (ester-urethane) s, I: Effect of varying polyester segment length. *Polymer* **53**, 3762–3771 (2012).
11. L. Hojabri, X.H. Kong, and S.S. Narine, Functional thermoplastics from linear diols and diisocyanates produced entirely from renewable lipid sources. *Biomacromolecules* **11**, 911–918 (2010).
12. A.L. Holmberg, K.H. Reno, R.P. Wool, and T.H. Epps III, Biobased building blocks for the rational design of renewable block polymers. *Soft Matter* **10**, 7405–7424 (2014).
13. L.H. Peebles, Hard block length distribution in segmented block copolymers. *Macromolecules* **9**, 58–61 (1976).
14. L. Peebles Jr., Sequence length distribution in segmented block copolymers. *Macromolecules* **7**, 872–882 (1974).
15. S. Shetranjiwalla, S. Li, L. Bouzidi, and S.S. Narine, Imparting elastomeric properties to entirely lipid-derived thermoplastic poly(ester urethane)s: Molecular weight control. *Polymer* **92**, 140–152 (2016).
16. L. Hojabri, X. Kong, and S.S. Narine, Fatty acid-derived diisocyanate and biobased polyurethane produced from vegetable oil: Synthesis, polymerization, and characterization. *Biomacromolecules* **10**, 884–891 (2009).
17. M.M. Coleman, K.H. Lee, D.J. Skrovanek, and P.C. Painter, Hydrogen bonding in polymers. 4. Infrared temperature studies of a simple polyurethane. *Macromolecules* **19**, 2149–2157 (1986).
18. R. Seymour, G. Estes, and S. Cooper, Infrared studies of segmented polyurethan elastomers. I. Hydrogen bonding. *Macromolecules* **3**, 579–583 (1970).
19. T. Pretsch, I. Jakob, and W. Müller, Hydrolytic degradation and functional stability of a segmented shape memory poly (ester urethane). *Polym. Degrad. Stab.* **94**, 61–73 (2009).
20. N. Murthy and H. Minor, General procedure for evaluating amorphous scattering and crystallinity from X-ray diffraction scans of semicrystalline polymers. *Polymer* **31**, 996–1002 (1990).
21. T. Ouchi, S. Nagasaka, and A. Hotta, β to α form transition observed in the crystalline structures of syndiotactic polystyrene (sPS). *Macromolecules* **44**, 2112–2119 (2011).
22. C. Fernández, M. Bermúdez, S. Muñoz-Guerra, S. León, R. Versteegen, and E. Meijer, Crystal structure and morphology of linear aliphatic n-polyurethanes. *Macromolecules* **43**, 4161–4171 (2010).

23. J. Mark, K. Ngai, W. Graessley, L. Mandelkern, E. Samulski, J. Koenig, and G. Wignall, *Physical Properties of Polymers*, ISBN 9780521530187, Cambridge University Press, Cambridge (2004).
24. A.I. Vogel, *Text-Book Of Practical Organic Chemistry*, Longmans Green, London, UK (1948).
25. A.S. More, T. Lebarbé, L. Maisonneuve, B. Gadenne, C. Alfos, and H. Cramail, Novel fatty acid based diisocyanates towards the synthesis of thermoplastic polyurethanes. *Eur. Polym. J.* **49**, 823–833 (2013).
26. R.L. McKiernan, S.P. Gido, and J. Penelle, Synthesis and characterization of polyethylene-like polyurethanes derived from long-chain, aliphatic α, ω-diols. *Polymer* **43**, 3007–3017 (2002).
27. R.W. Lenz, *Organic Chemistry of Synthetic High Polymers*, Interscience Wiley, New York (1967).
28. A. Mishra and P. Maiti, Morphology of polyurethanes at various length scale: The influence of chain structure. *J. Appl. Polym. Sci.* **120**, 3546–3555 (2011).
29. Y. Xu, Z. Petrovic, S. Das, and G.L. Wilkes, Morphology and properties of thermoplastic polyurethanes with dangling chains in ricinoleate-based soft segments. *Polymer* **49**, 4248–4258 (2008).
30. R. Poręba, J. Kredatusová, J. Hodan, M. Serkis, and M. Špírková, Thermal and mechanical properties of multiple-component aliphatic degradable polyurethanes. *J. Appl. Polym. Sci.* **132**, 41872(1–2) (2015).
31. M. Špírková, L. Machová, L. Kobera, J. Brus, R. Poręba, M. Serkis, and A. Zhigunov, Multiscale approach to the morphology, structure, and segmental dynamics of complex degradable aliphatic polyurethanes. *J. Appl. Polym. Sci.* **132**, 41590(1–11) (2015).
32. L.G. Lage and Y. Kawano, Thermal degradation of biomedical polyurethanes—A kinetic study using high-resolution thermogravimetry. *J. Appl. Polym. Sci.* **79**, 910–919 (2001).
33. Z.S. Petrović, Z. Zavargo, J.H. Flyn, and W.J. Macknight, Thermal degradation of segmented polyurethanes. *J. Appl. Polym. Sci.* **51**, 1087–1095 (1994).
34. K. Chrissafis, K. Paraskevopoulos, G. Papageorgiou, and D. Bikiaris, Thermal decomposition of poly (propylene sebacate) and poly (propylene azelate) biodegradable polyesters: Evaluation of mechanisms using TGA, FTIR and GC/MS. *J. Anal. Appl. Pyrol.* **92**, 123–130 (2011).
35. D. Chattopadhyay and D.C. Webster, Thermal stability and flame retardancy of polyurethanes. *Prog. Polym. Sci.* **34**, 1068–1133 (2009).
36. P. Król, Synthesis methods, chemical structures and phase structures of linear polyurethanes. Properties and applications of linear polyurethanes in polyurethane elastomers, copolymers and ionomers. *Prog. Mater. Sci.* **52**, 915–1015 (2007).
37. M.G. Menges, J. Penelle, C. Le Fevere de Ten Hove, A.M. Jonas, and K. Schmidt-Rohr, Characterization of long-chain aliphatic polyesters: Crystalline and supramolecular structure of PE22,4 elucidated by X-ray scattering and nuclear magnetic resonance. *Macromolecules* **40**, 8714–8725 (2007).
38. W.B. Liau and R.H. Boyd, Structure and packing in crystalline aliphatic polyesters. *Macromolecules* **23**, 1531–1539 (1990).
39. J. Zuo, S. Li, L. Bouzidi, and S.S. Narine, Thermoplastic polyester amides derived from oleic acid. *Polymer* **52**, 4503–4516 (2011).
40. H. Qi and M. Boyce, Stress–strain behavior of thermoplastic polyurethanes. *Mech. Mater.* **37**, 817–839 (2005).
41. G. Skarja and K. Woodhouse, Structure-property relationships of degradable polyurethane elastomers containing an amino acid-based chain extender. *J. Appl. Polym. Sci.* **75**, 1522–1534 (2000).
42. M. Kennedy, A. Peacock, and L. Mandelkern, Tensile properties of crystalline polymers: Linear polyethylene. *Macromolecules* **27**, 5297–5310 (1994).
43. L.T.J. Korley, B.D. Pate, E.L. Thomas, and P.T. Hammond, Effect of the degree of soft and hard segment ordering on the morphology and mechanical behavior of semicrystalline segmented polyurethanes. *Polymer* **47**, 3073–3082 (2006).

Supplementary Document Available Online

http://www.scrivenerpublishing.com/journalsuppl/jrm/JRM-2016-0061/jrm_JRM-2016-0061_supp1.docx